

Non-Hermitian Floquet topological phases in the double-kicked rotor

Longwen Zhou^{1,*} and Jiaxin Pan¹

¹*Department of Physics, College of Information Science and Engineering,
Ocean University of China, Qingdao, China 266100*

(Dated: 2022-03-18)

Dynamical kicking systems possess rich topological structures. In this work, we study Floquet states of matter in a non-Hermitian extension of double kicked rotor model. Under the on-resonance condition, we find various non-Hermitian Floquet topological phases, with each being characterized by a pair of topological winding numbers. A generalized mean chiral displacement is introduced to detect these winding numbers dynamically in two symmetric time frames. Furthermore, by mapping the system to a periodically quenched lattice model, we obtain the topological edge states and unravel the bulk-edge correspondence of the non-Hermitian double kicked rotor. These results uncover the richness of Floquet topological states in non-Hermitian dynamical kicking systems.

I. INTRODUCTION

Floquet topological phases of matter emerge in systems under time-periodic modulations. One class of Floquet systems that has been shown to possess rich topological properties are dynamical kicking systems [1]. They are first introduced in the study of dynamical localization and quantum chaos, with the kicked rotor (KR) been a prototypical example [2–7]. In 2008, Wang and Gong analyzed a modified version of the KR (also called double kicked rotor) [8], and discovered its fractal quasienergy spectrum that mimicking the Hofstadter butterfly in quantum Hall effects [9]. Later, rich Floquet topological states in the double kicked rotor (DKR) were characterized, and then employed to achieve quantized acceleration in momentum space [10]. The topological equivalence between the DKR and the kicked Harper model [11], another prototypical dynamical kicking system, has also been proved rigorously [12]. The introduction of a spin-1/2 degree of freedom to KR and DKR further uncovers the richness of Floquet topological states that can appear in dynamical kicking systems [13–15].

In the past decade, Floquet topological phases have attracted great interest across a broad range of research areas. This is mainly due to the richness and high-tunability of their topological properties [16–44], with potential applications in ultrafast electronics [45], quantum simulation [46] and quantum computing [47]. The topological classification of these dynamical states of matter also require new schemes [48–50] that go beyond their static cousins. Experimentally, Floquet topological phases have been realized in cold atom, photonic, phononic and acoustic systems [51–57].

In recent years, the study of Floquet topological phases has been extended to non-Hermitian domain [58, 59]. There, gain and loss or nonreciprocal effects were introduced to make the evolution of Floquet systems nonunitary [60–64]. In quantum walk setups, gain and loss

were implemented in several studies to measure the topological invariants [65–73]. Furthermore, a periodically quenched nonreciprocal lattice model has been found to possess abundant Floquet topological phases with arbitrarily many topological edge states induced by non-Hermitian effects [74]. In dynamical kicking systems, a \mathcal{PT} -symmetric kicked rotor was proposed [75, 76] and its transport properties have been investigated in [77]. However, the richness of non-Hermitian Floquet topological phases in dynamical kicking systems have not been revealed yet.

In this work, we introduce a DKR with complex kicking strengths, and unravel its fruitful non-Hermitian Floquet topological phases. After introducing our model in Sec. II, we analyze its spectrum, symmetry and topological properties in Sec. III. A pair of integer winding numbers is introduced to fully characterize the topological phases appearing in the non-Hermitian DKR. We further extend the definition of mean chiral displacement (MCD) to nonunitary evolution, and using it as a probe to extract the topological winding numbers of non-Hermitian DKR dynamically. By mapping our system to a periodically kicked lattice model, we also present its topological edge states under open boundary condition (OBC) and demonstrate its bulk-edge correspondence. We conclude our work and discuss potential future directions in Sec. IV.

II. THE MODEL

The DKR model is described by the Hamiltonian $\hat{H} = \frac{\hat{p}^2}{2} + \kappa_1 \cos(\hat{x} + \beta) \sum_{\ell \in \mathbb{Z}} \delta(t - \ell T) + \kappa_2 \cos(\hat{x}) \sum_{\ell \in \mathbb{Z}} \delta(t - \ell T - \tau)$. It can be realized by cold atoms subject to counter-propagating laser pulses in an optical lattice [78–80], where \hat{x} and \hat{p} are position and momentum operators of cold atoms. In a driving period T , the system is first kicked by a lattice potential of strength κ_1 . Then it is evolved freely over a time duration $\tau \in (0, T)$, kicked by another lattice potential of strength κ_2 , and then evolved freely over another time duration $T - \tau$. β is a controllable phase shift between the two kicking potentials.

* zhoulw13@u.nus.edu

The Floquet operator of DKR, obtained by integrating the Schrödinger equation $i\hbar\partial_t|\psi\rangle = \hat{H}|\psi\rangle$ over a complete driving period (e.g., from $t = \ell T - 0^+$ to $t = (\ell+1)T - 0^+$), is given by

$$\hat{U} = e^{-i(T-\tau)\frac{\hat{p}^2}{2\hbar}} e^{-i\frac{\kappa_2}{\hbar}\cos(\hat{x})} e^{-i\tau\frac{\hat{p}^2}{2\hbar}} e^{-i\frac{\kappa_1}{\hbar}\cos(\hat{x}+\beta)}. \quad (1)$$

In the Floquet operator, the spatial periodicity of kicking potentials allow the momentum \hat{p} to take eigenvalues $p = (n + \eta)\hbar$, where $n \in \mathbb{Z}$ and $\eta \in (0, 1)$ being the conserved quasimomentum. For a Bose-Einstein condensate of large coherence width, one can choose $\eta = 0$ [81, 82]. The momentum \hat{p} is then quantized as $\hat{p} = \hat{n}\hbar$, i.e., integer multiples of the effective Planck constant \hbar . Furthermore, under the condition $\hbar T = 4\pi$ [81–83], we obtain the on-resonance DKR (ORDKR) model, whose Floquet operator takes the form

$$\hat{U} = e^{+i\frac{\hbar\tau}{2}\hat{n}^2} e^{-iK_2\cos(\hat{x})} e^{-i\frac{\hbar\tau}{2}\hat{n}^2} e^{-iK_1\cos(\hat{x}+\beta)}. \quad (2)$$

Here $K_1 = \kappa_1/\hbar$ and $K_2 = \kappa_2/\hbar$ represent dimensionless kicking strengths. It has been shown that this ORDKR model possesses rich topological properties, including the Hofstadter butterfly-like Floquet spectrum [8], quasienergy bands with large Chern numbers, and quantized Thouless pumping in momentum space [10].

In this work, we further investigate the Floquet topological phases of ORDKR in non-Hermitian regime. More specifically, we will focus on the two-band situation by choosing the time delay τ between the two kicks such that $\hbar\tau = \pi$. The resulting non-Hermitian ORDKR (NH-ORDKR) model is described by the Floquet operator

$$\hat{U} = e^{i\frac{\pi}{2}\hat{n}^2} e^{-iK_2\cos(\hat{x})} e^{-i\frac{\pi}{2}\hat{n}^2} e^{-iK_1\cos(\hat{x}+\beta)}, \quad (3)$$

where the kicking strengths

$$K_j = u_j + iv_j \quad j = 1, 2 \quad (4)$$

now take complex values, with $\{u_1, v_1, u_2, v_2\} \in \mathbb{R}$. For an optical lattice, the imaginary parts of kicking strengths correspond to particle losses, which may be generated by using a resonant optical beam to kick the atoms out of the trap. It may also be realized by applying a radio frequency pulse to excite atoms to an irrelevant state, leading to an effective decay when atoms in that state experience a loss by applying an antitrap [84]. In photonic systems, a complex kicking strength correspond to a complex refractive index, whose imaginary part represents either loss or gain. This kind of potential has interesting engineering applications, such as realizing unidirectional transport of light [85] and other types of laser devices [63]. In the following, we will unravel rich Floquet topological phases in the NH-ORDKR induced by complex kicking lattice potentials.

III. FLOQUET TOPOLOGICAL PHASES IN NH-ORDKR

In this section, we first analysis the Floquet operator of NH-ORDKR in Eq. (3), and discuss the symmetry that protects its topological properties. Next, we investigate the quasienergy spectrum and the conditions of topological phase transitions in the NH-ORDKR. A pair of integer topological winding numbers is introduced to characterize each of its Floquet topological phases. To detect these winding numbers and distinguish different Floquet topological phases in the NH-ORDKR experimentally, we suggest to measure the MCD of a wave packet in the optical lattice. Finally, we map the Floquet operator of NH-ORDKR to a kicked lattice model in position representation, and uncover its Floquet edge states and bulk-edge correspondence under OBC.

A. Floquet operator and chiral symmetry

The Floquet operator of NH-ORDKR, as defined in Eq. (3), is translational invariant over two sites (i.e., $\hat{n} \rightarrow \hat{n} + 2$) in the momentum lattice. By introducing a bipartite lattice basis in momentum space and taking the periodic boundary condition, we could express the Floquet operator of NH-ORDKR as $\hat{U} = \sum_{\theta} U(\theta)|\theta\rangle\langle\theta|$, where

$$U(\theta) = e^{+i\frac{\pi}{4}\sigma_z} e^{-iK_2(\cos\frac{\theta}{2}\sigma_x + \sin\frac{\theta}{2}\sigma_y)} \times e^{-i\frac{\pi}{4}\sigma_z} e^{+iK_1(\cos\frac{\theta}{2}\sigma_x + \sin\frac{\theta}{2}\sigma_y)}, \quad (5)$$

and

$$K_1 \equiv K_1 \sin\frac{\theta}{2}, \quad K_2 \equiv K_2 \cos\frac{\theta}{2}, \quad (6)$$

with $\theta \in [-\pi, \pi)$ being the conserved quasiposition due to translational symmetry in momentum space, and $\sigma_{x,y,z}$ being Pauli matrices in their usual representation [see Appendix A for derivation details of Eq. (5)]. We have also set the phase delay between two kicks to be $\beta = \frac{\pi}{2}$, which allows $U(\theta)$ to possess nontrivial topological phases when $K_{1,2}$ taking real values [10].

To characterize the symmetry and topological properties of $U(\theta)$, we introduce a pair of symmetric time frames by resetting the start time of the evolution. In these time frames, $U(\theta)$ takes the form

$$U_1(\theta) = e^{-i\frac{\kappa_2}{2}(\cos\frac{\theta}{2}\sigma_x + \sin\frac{\theta}{2}\sigma_y)} e^{-iK_1(\sin\frac{\theta}{2}\sigma_x - \cos\frac{\theta}{2}\sigma_y)} \times e^{-i\frac{\kappa_2}{2}(\cos\frac{\theta}{2}\sigma_x + \sin\frac{\theta}{2}\sigma_y)}, \quad (7)$$

$$U_2(\theta) = e^{+i\frac{\kappa_1}{2}(\cos\frac{\theta}{2}\sigma_x + \sin\frac{\theta}{2}\sigma_y)} e^{-iK_2(\sin\frac{\theta}{2}\sigma_x - \cos\frac{\theta}{2}\sigma_y)} \times e^{+i\frac{\kappa_1}{2}(\cos\frac{\theta}{2}\sigma_x + \sin\frac{\theta}{2}\sigma_y)}. \quad (8)$$

Note that both $U_1(\theta)$ and $U_2(\theta)$ are similar to $U(\theta)$ (see

Appendix A for more details). Therefore, they share the same Floquet spectrum with $U(\theta)$ even if K_1 and K_2 are complex numbers. Furthermore, under the unitary transformation $\Gamma = \sigma_z$, we have

$$\Gamma U_\alpha(\theta) \Gamma = U_\alpha^{-1}(\theta) \quad \alpha = 1, 2, \quad (9)$$

which means that $U_1(\theta)$ and $U_2(\theta)$ have the chiral (sublattice) symmetry Γ . According to the symmetry classification of chiral symmetric Floquet systems in one-dimension [39] and its extension to non-Hermitian systems [74], each topological phase of $U(\theta)$ can be described by a pair of integer winding numbers extracted from $U_1(\theta)$ and $U_2(\theta)$. We will analyze the spectrum and topological properties of the NH-ORDKR in detail in the following subsections.

B. Quasienergy dispersion, topological invariants and phase diagram

Expanding $U_1(\theta)$ and $U_2(\theta)$ by the Euler formula, and recombining the resulting terms, we can express Eqs. (7) and (8) in a compact form as

$$U_\alpha(\theta) = e^{-iE(\theta)(n_{\alpha x}\sigma_x + n_{\alpha y}\sigma_y)}, \quad (10)$$

where $\alpha = 1, 2$ and

$$E(\theta) = \arccos(\cos \mathcal{K}_1 \cos \mathcal{K}_2) \quad (11)$$

gives the quasienergy dispersion relation $\pm E(\theta)$. Since the real part of $E(\theta)$ is only defined modulus 2π , the quasienergy spectrum gap closes when $\text{Im}E(\theta) = 0$ and $\text{Re}E(\theta) = 0$ or $\pm\pi$. When the spectrum becomes gapless, a topological phase transition may happen. Furthermore, $(n_{\alpha x}, n_{\alpha y})$ forms a complex-valued vector with $n_{\alpha x}^2 + n_{\alpha y}^2 = 1$ for $\alpha = 1, 2$ (see Appendix B for more details). Using these vectors, we can define a winding number for $U_\alpha(\theta)$ as

$$\nu_\alpha = \int_{-\pi}^{\pi} \frac{d\theta}{2\pi} (\mathbf{n}_\alpha \times \partial_\theta \mathbf{n}_\alpha)_z, \quad \alpha = 1, 2. \quad (12)$$

It is not hard to see that ν_α take real values, as the imaginary part of $\mathbf{n}_\alpha \equiv (n_{\alpha x}, n_{\alpha y})$ has no winding in the Brillouin zone [74]. Then, following the description of chiral symmetric non-Hermitian Floquet systems [74], the topological phases of $U(\theta)$ can be characterized by a pair of integer winding numbers, given by [86]

$$\nu_0 = \frac{\nu_1 + \nu_2}{2}, \quad \nu_\pi = \frac{\nu_1 - \nu_2}{2}. \quad (13)$$

In the Hermitian limit (imaginary parts of the two kicking strengths $v_1 = v_2 = 0$), ν_0 and ν_π also predict the number of topological edge modes at quasienergy zero and π in the ORDKR model [10].

In the following, we will analyze the spectrum and

topological phases of ORDKR under three representative non-Hermitian kicking potentials: (i) $v_1 \neq 0, v_2 = 0$ or vice versa; (ii) $v_1 = v_2 = v \neq 0$; and (iii) $v_1 \neq v_2$ with $v_1, v_2 \neq 0$. In each case, we give the condition of topological phase transition, computing winding numbers for each of the topological phases, and constructing the corresponding topological phase diagram.

1. Case (i)

We first consider the case when only one of the kicking strengths (K_1 or K_2) in Eq. (4) is complex. Under the gapless condition $\cos[E(\theta)] = \pm 1$, it can be shown that if $v_1 \neq 0$ and $v_2 = 0$, u_1, u_2 and v_1 in Eq. (4) satisfy the equation (see Appendix C for derivation details):

$$v_1 = \frac{u_1}{n\pi} \text{arccosh} \left[\frac{\pm 1}{\cos \left(u_2 \sqrt{1 - \frac{n^2 \pi^2}{u_1^2}} \right)} \right], \quad n \in \mathbb{Z}. \quad (14)$$

Similarly, if $v_2 \neq 0$ and $v_1 = 0$, the gapless condition yields

$$v_2 = \frac{u_2}{n\pi} \text{arccosh} \left[\frac{\pm 1}{\cos \left(u_1 \sqrt{1 - \frac{n^2 \pi^2}{u_2^2}} \right)} \right], \quad n \in \mathbb{Z}. \quad (15)$$

Note that Eqs. (14) and (15) are symmetric under the exchange of subindices $1 \leftrightarrow 2$. So we can focus on the non-Hermitian Floquet topological phases and phase transitions related to only one of them without loss of generality.

To check whether a non-vanishing imaginary part of K_1 or K_2 could induce new topological phases in the NH-ORDKR, we need to investigate the behavior of winding numbers Eq. (12) versus this imaginary part. A representative example is shown in Fig. 1, where we choose $u_1 = 0.5\pi$ and $u_2 = 5.5\pi$ for the real parts of kicking strengths. According to Ref. [10], this choice leads to a Floquet topological phase with $(\nu_0, \nu_\pi) = (2, 3)$ in the Hermitian limit. In Fig. 1, we observe that with the increase of imaginary kicking strength v_2 , a series of topological phase transitions happen at $v_2 = p_n$ with $n = 1, \dots, 5$ in Eq. (15). Each transition is accompanied by the vanishing of a spectrum gap, together with the quantized change of winding number ν_0 (blue solid line) or ν_π (red dashed line) by 1. In the limit $v_2 \rightarrow \infty$, the system ends in a topologically trivial phase with $\nu_0 = \nu_\pi = 0$.

Therefore, we conclude that a non-vanishing imaginary part in the kicking strength K_1 or K_2 of the NH-ORDKR could indeed induce topological phase transitions and create non-Hermitian Floquet topological phases, with each characterized by a pair of integer quantized winding numbers (ν_0, ν_π) . In more general situations, analytical solutions for the gap closing conditions like Eqs. (14) and (15) may not be available. We will consider these cases

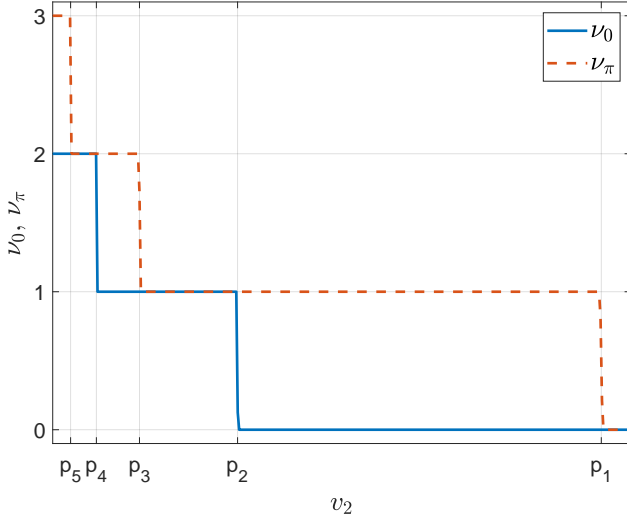


FIG. 1. Evolution of the winding numbers ν_0 (blue solid line) and ν_π (red dashed line) vs. the imaginary part of the kicking strength $K_2 = u_2 + iv_2$. System parameters are chosen as $u_1 = 0.5\pi$ and $u_2 = 5.5\pi$ and $v_1 = 0$. The numerical values of p_1, p_2, p_3, p_4, p_5 along the v -axis are obtained analytically from Eq. (15) with $n = 1, 2, 3, 4, 5$.

in the following.

2. Case (ii)

In this case, both the two kicking strengths K_1 and K_2 take complex values under the constraint that their imaginary parts are equal, i.e., $v_1 = v_2 = v$. Using the gapless condition (see Appendix C for more details) and the winding numbers (ν_0, ν_π) , we could then numerically characterize the Floquet topological phases of NH-ORDKR at different imaginary kicking strength v . Two representative examples will be discussed as follows.

In the first example, we choose $u_1 = 6.5\pi$ and $u_2 = 0.5\pi$ for the real parts of two kicking strengths. When $v = 0$, the system is in a Hermitian Floquet topological phase with $\nu_0 = \nu_\pi = 3$. As shown in Fig. 2, increasing the imaginary kicking strength v yields consecutive Floquet topological phase transitions. Each transition happens when one of the gap functions (Δ_0, Δ_π) [see Eqs. (C8) and (C9)] vanishes, accompanied by a quantized change of ν_0 or ν_π by 1. In the limit $v \rightarrow \infty$, the system becomes topologically trivial, with $\nu_0 = \nu_\pi = 0$. Similar patterns of topological phase transitions are observed by exchanging the values of u_1 and u_2 for the two kicking strengths.

In the second example, we take $u_1 = u_2 = u$, which further indicates that $K_1 = K_2$. Plugging this condition into Eq. (13), we will always have $\nu_1 = \nu_2$. Therefore, we can obtain the topological phase diagram of the NH-ORDKR versus u and v , with each phase characterized only by ν_0 . A representative portion of the phase diagram is shown in Fig. 3. Interestingly, we see that the increase

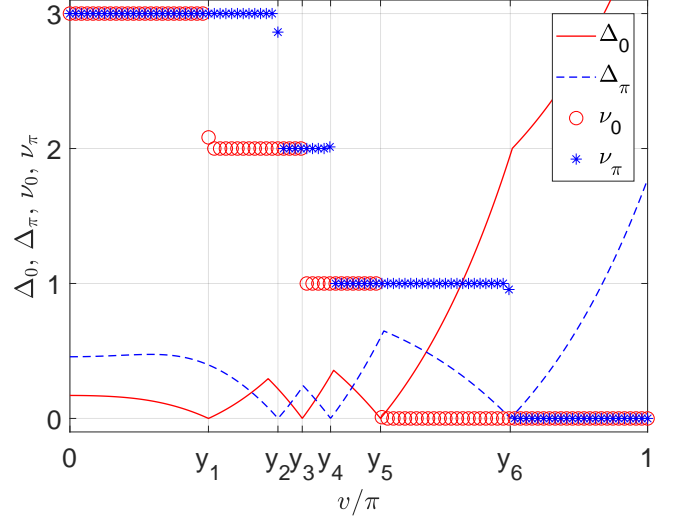


FIG. 2. Evolution of quasienergy gap functions Δ_0 (red solid line), Δ_π (blue dashed line) [see Eqs. (C8) and (C9) for the definitions] and winding numbers ν_0 (red circles) and ν_π (blue stars) vs. the imaginary parts of kicking strengths $K_1 = u_1 + iv$ and $K_2 = u_2 + iv$. System parameters are chosen as $u_1 = 6.5\pi$ and $u_2 = 0.5\pi$. The numerical values of y_1, y_3, y_5 (y_2, y_4, y_6) along the v -axis are obtained by searching the local minimum of the gap function Δ_0 (Δ_π) around quasienergy $E = 0$ ($E = \pi$).

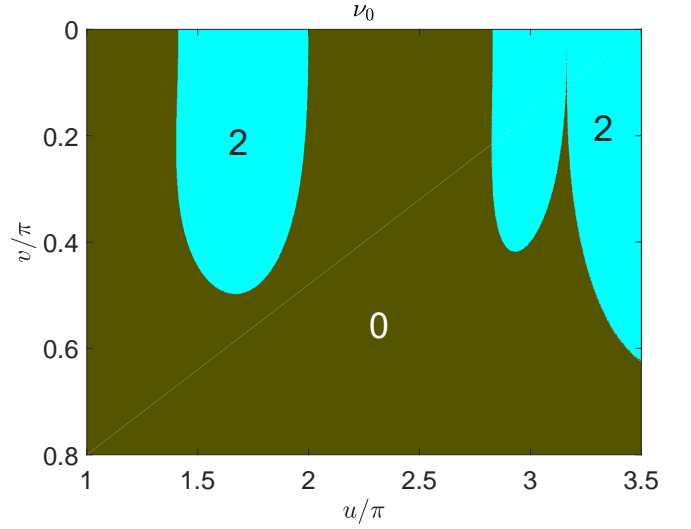


FIG. 3. The topological phase diagram of NH-ORDKR vs. real and imaginary parts of kicking strengths $K_1 = K_2 = u + iv$. Each region with a uniform color corresponds to a Floquet topological phase of the NH-ORDKR, with the numerical value of winding number ν_0 shown in the panel.

of u and v could both induce topological phase transitions in the NH-ORDKR. This further reveal the possibility of generating rich Floquet topological states in the ORDKR by complex kicking potentials.

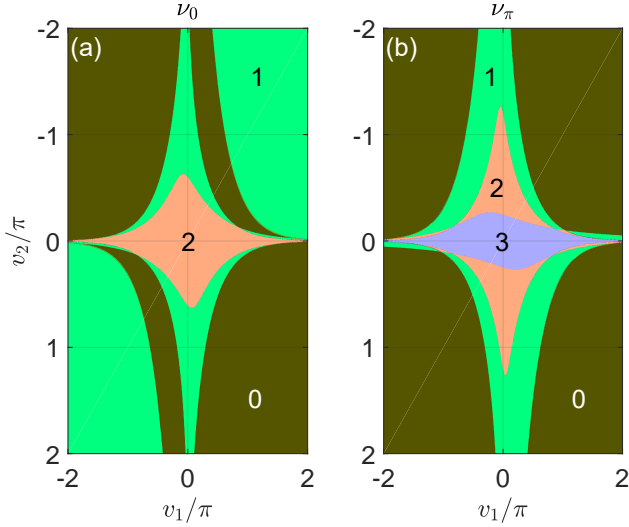


FIG. 4. The topological phase diagram of NH-ORDKR vs. imaginary parts of kicking strengths $K_1 = u_1 + iv_1$ and $K_2 = u_2 + iv_2$. System parameters are chosen as $u_1 = 0.5\pi$ and $u_2 = 5.5\pi$. In panel (a) [(b)], each region with a uniform color corresponds to a Floquet topological phase of the NH-ORDKR, with the numerical value of winding number ν_0 (ν_π) shown in the panel.

3. Case (iii)

In this case, we allow both K_1 and K_2 to be complex, with no constraint on their imaginary parts. The resulting topological phase diagram versus v_1 and v_2 , with $(u_1, u_2) = (0.5\pi, 5.5\pi)$ and $(u_1, u_2) = (5.5\pi, 0.5\pi)$ are shown in Figs. 4 and 5, respectively. In each phase diagram, the panels (a) and (b) correspond to the values of winding numbers ν_0 and ν_π , respectively. A region with a uniform color refers to a parameter domain in which ν_0 [panel (a)] or ν_π [panel (b)] take the same value. We see that with the change of v_1 and v_2 , a couple of non-Hermitian Floquet topological phases are induced, with each characterized by the winding numbers (ν_0, ν_π) . Across the boundary between two topological phases, a quantized change of ν_0 or ν_π is observed, which indicates the existence of a topological phase transition.

To sum up, we find that topological phase transitions are generic in the NH-ORDKR model, and rich non-Hermitian Floquet topological phases could emerge under the effect of complex kicking potentials. In the following subsection, we will introduce a dynamical indicator – the MCD – to detect the winding numbers of these non-Hermitian Floquet topological phases.

C. MCD and winding numbers

The MCD describes the shift of a localized wave packet in a bipartite lattice over a long time duration. It is proposed as a way to detect the winding num-

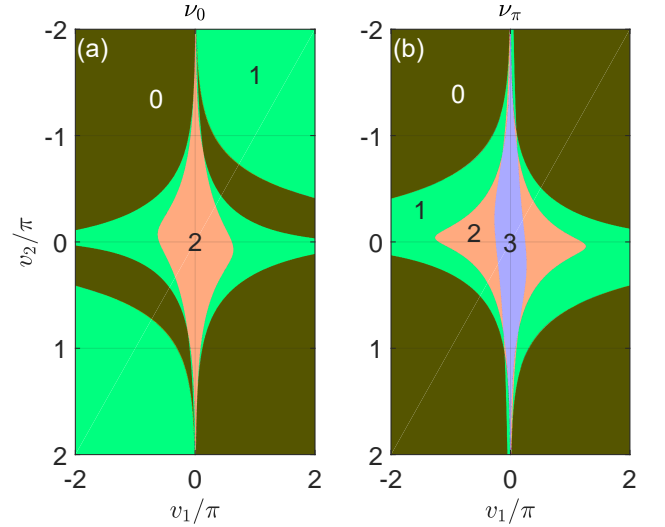


FIG. 5. The topological phase diagram of NH-ORDKR vs. imaginary parts of kicking strengths $K_1 = u_1 + iv_1$ and $K_2 = u_2 + iv_2$. System parameters are chosen as $u_1 = 5.5\pi$ and $u_2 = 0.5\pi$. In panel (a) [(b)], each region with a uniform color corresponds to a Floquet topological phase of the NH-ORDKR, with the numerical value of winding number ν_0 (ν_π) shown in the panel.

bers of chiral symmetric topological insulators in one-dimension [87, 88]. In later studies, the MCD is applied to extract the winding numbers of Floquet systems [15] and also extended to two-dimensional systems with higher order topological states [89]. In this work, we generalize the MCD to non-Hermitian chiral symmetric Floquet systems, and using it as a dynamical probe to the winding numbers of NH-ORDKR.

For a non-Hermitian Floquet system with chiral symmetry Γ , we define the chiral displacement as

$$C_\alpha(t) \equiv \text{Tr} \left(\rho_0 \hat{U}_\alpha^{\dagger t} (\hat{n} \otimes \Gamma) \hat{U}_\alpha^t \right), \quad (16)$$

where $\alpha = 1, 2$ is the index of symmetric time frame, t is the number of driving periods, and \hat{n} is the unit cell position operator (or momentum operator if the lattice is in momentum space). The initial state $\rho_0 = \frac{|0\rangle\langle 0| \otimes \sigma_0}{2}$ describes a uniform mixture of sublattice eigenstates $|a\rangle$ and $|b\rangle$ in the 0's unit cell of the lattice. The choice of ρ_0 here is different from the case in Hermitian limit, in which the initial state occupies only a single sublattice in the 0's unit cell. Furthermore, the Floquet operator \hat{U}_α is different from \hat{U} (the Floquet operator of the system in the α 's time frame), in the sense that if $|\psi\rangle$ is a right eigenvector of \hat{U}_α with quasienergy E , then it is a left eigenvector of \hat{U}_α with the same quasienergy.

With these definitions and after relatively straightforward calculations (see Appendix D for more details), the

(normalized) MCD in long-time limit is given by

$$\bar{C}_\alpha = \lim_{t \rightarrow \infty} \frac{1}{t} \sum_{t'=1}^t \int_{-\pi}^{\pi} \frac{d\theta}{2\pi} \frac{(\mathbf{n}_\alpha \times \partial_\theta \mathbf{n}_\alpha)_z}{1 + |\cot(Et')|^2} \quad (17)$$

$$= \frac{\nu_\alpha}{2}.$$

Here $\mathbf{n}_\alpha = (n_{\alpha x}, n_{\alpha y})$ is the winding vector of Floquet operator in the α 's time frame ($\alpha = 1, 2$). For the NH-ORDKR, explicit expressions of $(n_{\alpha x}, n_{\alpha y})$ are given by Eqs. (B3) to (B6) in Appendix B. Note that a normalization factor is introduced during the derivation of Eq. (17), which helps to cancel the effects of gain/loss on the amplitude of the evolving state. To reach the second equality of Eq. (17), we notice that $\frac{1}{1 + |\cot(Et')|^2} = \frac{1}{2}(1 - \cos[2\text{Re}(E)t'] / \cosh[2\text{Im}(E)t'])$. When $\text{Im}(E) = 0$, we have an oscillating factor $\frac{1}{2}(1 - \cos[2\text{Re}(E)t'])$, which will be averaged to $\frac{1}{2}$ under $\lim_{t \rightarrow \infty} \frac{1}{t} \sum_{t'=1}^t$. When $\text{Im}(E) \neq 0$, the ratio $\cos[2\text{Re}(E)t'] / \cosh[2\text{Im}(E)t']$ will approach 0 quickly at large t' , leaving only a factor $\frac{1}{2}$ in $\frac{1}{1 + |\cot(Et')|^2}$. Therefore, we have $\lim_{t \rightarrow \infty} \frac{1}{t} \sum_{t'=1}^t \frac{1}{1 + |\cot(Et')|^2} \rightarrow \frac{1}{2}$, and the other terms under the integral of Eq. (17) gives nothing but the winding number ν_α . The winding numbers (ν_0, ν_π) can then be obtained from \bar{C}_α as

$$\nu_0 = |\bar{C}_1 + \bar{C}_2|, \quad \nu_\pi = |\bar{C}_1 - \bar{C}_2|. \quad (18)$$

Importantly, even though the dispersion $E(\theta)$ of NH-ORDKR is complex-valued in general, the MCD as defined in Eq. (16) could still capture the topological winding numbers of the system dynamically, which emphasize its generality as a tool in probing non-Hermitian topological phases with chiral symmetry.

In Fig. 6, we show the winding number ν_0 (solid line) and ν_π (dashed line) of NH-ORDKR calculated by the theoretical Eqs. (12) and (13), together with $|\bar{C}_1 + \bar{C}_2|$ (\bar{C}_0 in the figure, denoted by circles) and $|\bar{C}_1 - \bar{C}_2|$ (\bar{C}_π in the figure, denoted by triangles) calculated numerically by Eq. (17). Other system parameters are chosen as $u_1 = 5.5\pi, u_2 = 0.5\pi$ and $v_2 = 0$. It is clear that the theoretical predictions of (ν_0, ν_π) and numerical results of MCD are well consistent with each other, which verifies Eq. (18).

In Fig. 7, we give another example of MCD versus winding numbers, in which the system parameters are $u_1 = 0.5\pi, u_2 = 6.5\pi$ and the imaginary parts of the two kicking strengths are equal. In this case, we again observe nice consistency between the MCD and winding numbers of NH-ORDKR within each of its topological phases. Therefore, we conclude that the MCD, as defined by Eq. (17), can be used as a generic probe to the topological winding numbers and topological phase transitions of one-dimensional non-Hermitian Floquet systems with chiral symmetry. To detect MCD in experiments, one may first prepare the mixed state ρ_0 with zero momentum, and then evolve it in two different symmetric time frames and measure the shift of its center over differ-

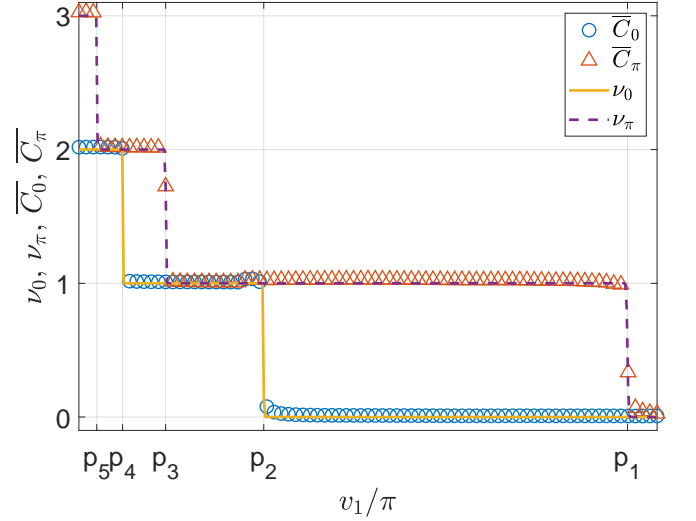


FIG. 6. The MCD $\bar{C}_0 = |\bar{C}_1 + \bar{C}_2|$ (blue circles), $\bar{C}_\pi = |\bar{C}_1 - \bar{C}_2|$ (red triangles) and winding numbers ν_0 (yellow solid line), ν_π (purple dashed line) vs. the imaginary part of kicking strength $K_1 = u_1 + iv_1$. System parameters are set as $u_1 = 5.5\pi, K_2 = u_2 = 0.5\pi$, and the results for \bar{C}_0, \bar{C}_π are averaged over $t = 50$ kicking periods. $v_1 = p_5$ to p_1 correspond to gap closing points obtained from Eq. (14) with $n = 5, 4, 3, 2, 1$.

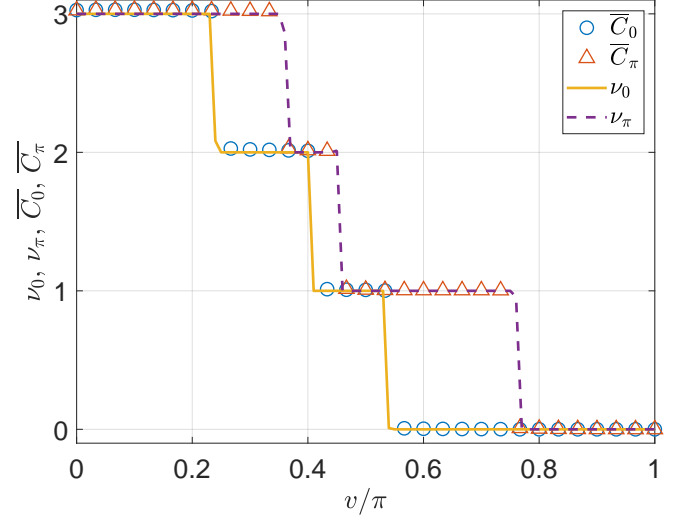


FIG. 7. The MCD $\bar{C}_0 = |\bar{C}_1 + \bar{C}_2|$ (blue circles), $\bar{C}_\pi = |\bar{C}_1 - \bar{C}_2|$ (red triangles) and winding numbers ν_0 (yellow solid line), ν_π (purple dashed line) vs. the imaginary part of kicking strengths $K_1 = u_1 + iv$ and $K_2 = u_2 + iv$. System parameters are set as $u_1 = 0.5\pi, u_2 = 6.5\pi$, and the results for \bar{C}_0, \bar{C}_π are averaged over $t = 50$ kicking periods.

ent number of driving periods in each time frame. Eqs. (18) and (17) can then be used to predict the topological winding numbers of the corresponding non-Hermitian Floquet system.

D. Edge states and bulk-edge correspondence

The bulk-edge correspondence relates the number of topological edge states to the bulk topological invariant of the considered system. It forms an important recipe in the characterization of topological phases both theoretically and experimentally. The bulk-edge correspondence in non-Hermitian systems can be more complicated [90, 91] due to the existence of high-order exceptional points [92, 93] and the so-called non-Hermitian skin effect [94]. In an earlier study, it has been shown that the bulk-edge correspondence can be recovered in non-Hermitian Floquet systems under appropriate conditions [74]. Below we demonstrate that the bulk-edge correspondence also hold in the NH-ORDKR.

For the ORDKR, the lattice is defined in momentum space, where it is not straightforward to take an OBC and investigate the properties of edge states. To study the bulk-edge correspondence in the NH-ORDKR, we can map its Hamiltonian to a periodically quenched lattice in position space. The resulting Floquet operator, according to Eqs. (A8) – (A10) in Appendix A, can be expressed as

$$\begin{aligned} \hat{U} = & e^{+i\frac{\pi}{4} \sum_n |n\rangle\langle n| \sigma_z} e^{-i\frac{K_2}{2} \sum_n (|n\rangle\langle n| \sigma_+ + |n\rangle\langle n+1| \sigma_- + \text{h.c.})} \\ & \times e^{-i\frac{\pi}{4} \sum_n |n\rangle\langle n| \sigma_z} e^{-i\frac{K_1}{2} \sum_n i(|n\rangle\langle n| \sigma_+ + |n\rangle\langle n+1| \sigma_- - \text{h.c.})}, \end{aligned} \quad (19)$$

where n is now interpreted as the unit cell index of a real space lattice, and the Pauli matrices operate in the space of its sublattices. In this periodically quenched lattice model, the complex potentials K_1 and K_2 can be realized by introducing nonreciprocal hoppings and onsite gain/loss inside a unit cell and among nearest neighbor unit cells. The implementation of these effects should be within reach in current photonic-based experimental setups [95].

The quasienergy spectrum and edge states of \hat{U} can now be obtained by solving the Floquet eigenvalue equation $\hat{U}|\psi\rangle = e^{-iE}|\psi\rangle$ under the OBC. In Fig. 8, we show the Floquet spectrum of \hat{U} for $u_1 = 5.5\pi$, $u_2 = 0.5\pi$ and $v_1 = v_2 = v$. In the lower panel, we observe edge states pinned at quasienergies 0 and π in different regimes of the parameter space, with their numbers change when the quasienergy gap closes at $E = 0$ or $E = \pm\pi$.

In Fig. 9, we further show the number of topological edge states n_0 at quasienergy 0 (red solid line) and n_π at quasienergy $\pm\pi$ (blue dashed line) by computing the inverse participation ratio, with the same parameter choices as in Fig. 8. $y_1 \sim y_5$ along the v -axis correspond to the gap closing points of the bulk quasienergy spectrum obtained from Eq. (11). We see that each time when the gap closes at quasienergy 0 (π), n_0 (n_π) will get a quantized change by 2, corresponding to a topological phase transition with winding number ν_0 (ν_π) changing by 1. In other regions, the bulk-edge correspondence de-

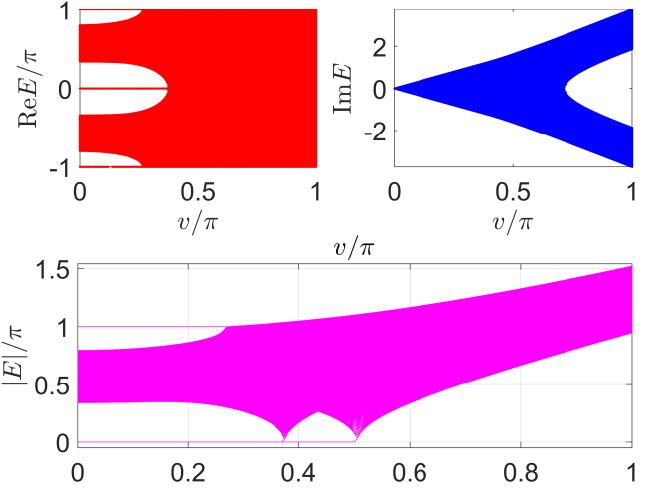


FIG. 8. Floquet spectrum of the NH-ORDKR vs. v under OBC for kicking strengths $K_1 = 5.5\pi + iv$ and $K_2 = 0.5\pi + iv$. The number of unit cells is chosen as $N = 4000$ in the calculation.

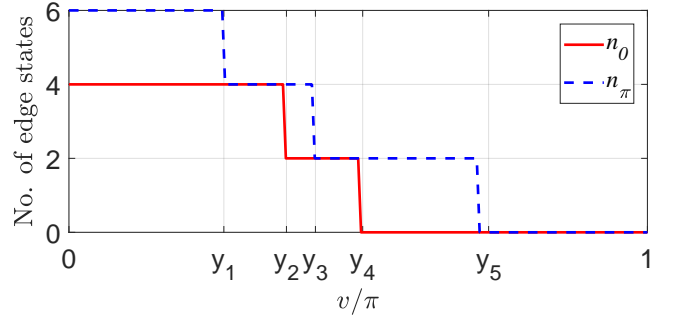


FIG. 9. Number of edge states at quasienergies 0 (n_0) and $\pm\pi$ (n_π) vs. the imaginary parts of kicking strengths $K_1 = u_1 + iv_1$ and $K_2 = u_2 + iv_2$ in the NH-ORDKR. System parameters are chosen as $u_1 = 5.5\pi$, $u_2 = 0.5\pi$ and $v_1 = v_2 = v$. The number of unit cells is $N = 4000$. The bulk Floquet spectrum is gapless at quasienergy 0 or π when $v = y_1, y_2, y_3, y_4, y_5$, as obtained from the conditions (C8) and (C9).

scribed by the relations

$$n_0 = 2\nu_0, \quad n_\pi = 2\nu_\pi, \quad (20)$$

hold as in Hermitian Floquet systems, with a small deviation around y_5 due to finite size effects. Eq. (20) has also been checked numerically in other parameter regimes of the NH-ORDKR, with similar results obtained. Therefore, we conclude that the bulk-edge correspondence in the NH-ORDKR, as described by Eq. (20) holds in the same way as in the Hermitian ORDKR. Experimentally, the non-Hermitian Floquet topological edge states have been observed in photonic quantum walks [95]. We expect the relation (20) of NH-ORDKR to be verifiable in similar experimental setups.

IV. CONCLUSIONS

In this work, we investigated Floquet topological phases in a non-Hermitian extension of the double kicked rotor, which is a prototypical example of dynamical kicking systems. Under the on resonance condition, the system possesses rich non-Hermitian Floquet topological phases protected by chiral symmetry. The topological phase diagram of the NH-ORDKR is obtained, with each of its phase being characterized by a pair of integer winding numbers. These winding numbers could be detected dynamically by measuring the mean chiral displacement in two symmetric time frames. Furthermore, by mapping our model to a periodically quenched lattice, we found its topological edge states. The number of these states at quasienergies 0 and $\pm\pi$ in each topological phase is precisely counted by the winding numbers of bulk states, revealing the bulk-edge correspondence of the NH-ORDKR.

In future studies, more fruitful topological structures are expected to appear in non-Hermitian dynamical kicking systems after introducing spin degrees of freedom and many-body interactions. Interesting examples include the recently discovered Floquet non-Hermitian skin effect [96] in momentum space and the non-Hermitian counterpart of Floquet topological time crystals [47]. New schemes that go beyond the existing 38-fold way for classification of static non-Hermitian topological phases [97, 98] should be required to achieve a full characterization of these non-Hermitian Floquet states [99]. On application side, the mean chiral displacement proposed in this work could assist the future experimental detection of topological invariants in non-Hermitian Floquet systems. Furthermore, with the promising proposal of Floquet topological quantum computing [47] and Floquet quantum state transfer [100], it would be interesting to investigate the potential of the Floquet topological edge states found in this work in achieving quantum computing and quantum information transfer against environmental effects that can be modeled by non-Hermitian Hamiltonians.

ACKNOWLEDGEMENT

L. Z. acknowledges Jiangbin Gong and Bo Qu for helpful comments. This work is supported by the National Natural Science Foundation of China (Grant No. 11905211), the Young Talents Project at Ocean University of China (Grants No. 861801013196 and 841912009) and the Applied Research Project of Postdoctoral Fellows in Qingdao (Grant No. 861905040009).

Appendix A: Floquet operator in different representations

The Floquet operator of NH-ORDKR, as given by Eq. (3) in the main text, can be expressed in the momentum lattice representation as follows. We first write out its component terms as

$$e^{\pm i \frac{\pi}{2} \hat{n}^2} \quad (A1)$$

$$= e^{\pm i \frac{\pi}{4}} e^{\pm i \frac{\pi}{4} \sum_{\ell} (|2\ell-1\rangle\langle 2\ell-1| - |2\ell\rangle\langle 2\ell|)},$$

$$e^{-i K_1 \cos(\hat{x} + \beta)} \quad (A2)$$

$$= e^{-i \frac{K_1}{2} \sum_{\ell} (e^{i\beta} |2\ell-1\rangle\langle 2\ell| + e^{i\beta} |2\ell\rangle\langle 2\ell+1| + \text{h.c.})},$$

$$e^{-i K_2 \cos(\hat{x})} \quad (A3)$$

$$= e^{-i \frac{K_2}{2} \sum_{\ell} (|2\ell-1\rangle\langle 2\ell| + |2\ell\rangle\langle 2\ell+1| + \text{h.c.})},$$

where the resolution identity $I = \sum_{\ell} |\ell\rangle\langle\ell|$ has been inserted to arrive at the expansions. Since Eq. (3) is invariant under the translation over two sites in momentum space, we could decompose the momentum space lattice into two chains containing only odd and even sites, denoted by sublattice indices a and b , respectively. A unit cell of the momentum space lattice now contains two sublattice sites, and we can introduce Pauli matrices in the sublattice representation as

$$\sigma_x = |a\rangle\langle b| + |b\rangle\langle a|, \quad (A4)$$

$$\sigma_y = i(|b\rangle\langle a| - |a\rangle\langle b|), \quad (A5)$$

$$\sigma_z = |a\rangle\langle a| - |b\rangle\langle b|. \quad (A6)$$

The sublattice raising and lower operators can also be expressed as

$$\sigma_{\pm} = \frac{\sigma_x + i\sigma_y}{2}. \quad (A7)$$

In this bipartite lattice representation, Eqs. (A1) to (A3) can be written as

$$e^{\pm i \frac{\pi}{2} \hat{n}^2} = e^{\pm i \frac{\pi}{4}} e^{\pm i \frac{\pi}{4} \sum_n |n\rangle\langle n| \sigma_z} \quad (A8)$$

$$e^{-i K_1 \cos(\hat{x} + \beta)} \quad (A9)$$

$$= e^{-i \frac{K_1}{2} \sum_n (e^{i\beta} |n\rangle\langle n| \sigma_+ + e^{i\beta} |n\rangle\langle n+1| \sigma_- + \text{h.c.})},$$

$$e^{-i K_2 \cos(\hat{x})} \quad (A10)$$

$$= e^{-i \frac{K_2}{2} \sum_n (|n\rangle\langle n| \sigma_+ + |n\rangle\langle n+1| \sigma_- + \text{h.c.})},$$

where n is the unit cell index. Performing the Fourier transforms $|n\rangle = \sum_{\theta} e^{-in\theta} |\theta\rangle$, $\langle n| = \sum_{\theta} e^{in\theta} \langle\theta|$ to Eqs.

(A8) to (A10) and choosing $\beta = \frac{\pi}{2}$, we arrive at

$$e^{\pm \frac{\pi}{2} \hat{n}^2} = e^{\pm i \frac{\pi}{4}} e^{\pm i \frac{\pi}{4} \sum_{\theta} |\theta\rangle \langle \theta| \sigma_z} \quad (\text{A11})$$

$$e^{-i K_1 \cos(\hat{x} + \beta)} \quad (\text{A12})$$

$$= e^{-i \frac{K_1}{2} \sum_{\theta} |\theta\rangle \langle \theta| (i \sigma_+ + i e^{i\theta} \sigma_- + \text{h.c.})},$$

$$e^{-i K_2 \cos(\hat{x})} \quad (\text{A13})$$

$$= e^{-i \frac{K_2}{2} \sum_{\theta} |\theta\rangle \langle \theta| (\sigma_+ + e^{i\theta} \sigma_- + \text{h.c.})}.$$

Combing these terms in sequential order and using Eq. (A7), we obtain the Floquet operator of NH-ORDKR in the form $\hat{U} = \sum_{\theta} U(\theta) |\theta\rangle \langle \theta|$, with

$$U(\theta) = e^{+i \frac{\pi}{4} \sigma_z} e^{-i \frac{K_2}{2} [(1 + \cos \theta) \sigma_x + \sin \theta \sigma_y]} \\ \times e^{-i \frac{\pi}{4} \sigma_z} e^{+i \frac{K_1}{2} [\sin \theta \sigma_x + (1 - \cos \theta) \sigma_y]} \quad (\text{A14})$$

Finally, using trigonometric relations $\sin \theta = 2 \sin \frac{\theta}{2} \cos \frac{\theta}{2}$ and $\cos \theta = 2 \cos^2 \frac{\theta}{2} - 1 = 1 - 2 \sin^2 \frac{\theta}{2}$, we arrive at Eq. (5) of the main text.

$U(\theta)$ can be further expressed in the two symmetric time frames as discussed in the main text. To do so, we first shift the starting time of the evolution to the start of the second half of driving period, and split the kick $e^{-i \frac{K_2}{2} [(1 + \cos \theta) \sigma_x + \sin \theta \sigma_y]}$ into two “half kicks” at the start and end of the shifted evolution. The resulting Floquet operator in this new time frame is given by

$$U_1(\theta) = e^{-i \frac{K_2}{2} (\cos \frac{\theta}{2} \sigma_x + \sin \frac{\theta}{2} \sigma_y)} \\ \times e^{-i \frac{\pi}{4} \sigma_z} e^{+i K_1 (\cos \frac{\theta}{2} \sigma_x + \sin \frac{\theta}{2} \sigma_y)} e^{+i \frac{\pi}{4} \sigma_z} \quad (\text{A15})$$

$$\times e^{-i \frac{K_2}{2} (\cos \frac{\theta}{2} \sigma_x + \sin \frac{\theta}{2} \sigma_y)}.$$

Similarly, by splitting $e^{+i K_1 (\cos \frac{\theta}{2} \sigma_x + \sin \frac{\theta}{2} \sigma_y)}$ into two “half kicks” and shifting one of them to the end of the evolution, $U(\theta)$ in Eq. (A14) becomes

$$U_2(\theta) = e^{+i \frac{K_1}{2} (\cos \frac{\theta}{2} \sigma_x + \sin \frac{\theta}{2} \sigma_y)} \\ \times e^{+i \frac{\pi}{4} \sigma_z} e^{-i K_2 (\cos \frac{\theta}{2} \sigma_x + \sin \frac{\theta}{2} \sigma_y)} e^{-i \frac{\pi}{4} \sigma_z} \quad (\text{A16})$$

$$\times e^{+i \frac{K_1}{2} (\cos \frac{\theta}{2} \sigma_x + \sin \frac{\theta}{2} \sigma_y)}.$$

It is clear that both $U_1(\theta)$ and $U_2(\theta)$ are related to $U(\theta)$ by similarity transformations. Finally, using the transformations $e^{\mp i \frac{\pi}{4} \sigma_z} \sigma_x e^{\pm i \frac{\pi}{4} \sigma_z} = \pm \sigma_y$ and $e^{\mp i \frac{\pi}{4} \sigma_z} \sigma_y e^{\pm i \frac{\pi}{4} \sigma_z} = \mp \sigma_x$, Eqs. (A15) and (A16) simplify to Eqs. (7) and (8) in the main text.

Appendix B: Explicit expressions of the Floquet operators

Using the Euler formula $e^{i \phi \mathbf{n} \cdot \boldsymbol{\sigma}} = \cos \phi + i \sin \phi \mathbf{n} \cdot \boldsymbol{\sigma}$, we can expand each exponential of Eqs. (7) and (8) in the main text. The resulting terms can be recombined

to give

$$U_1(\theta) = \cos \mathcal{K}_1 \cos \mathcal{K}_2 \quad (\text{B1})$$

$$-i \left[\cos \frac{\theta}{2} \cos \mathcal{K}_1 \sin \mathcal{K}_2 + \sin \frac{\theta}{2} \sin \mathcal{K}_1 \right] \sigma_x$$

$$-i \left[\sin \frac{\theta}{2} \cos \mathcal{K}_1 \sin \mathcal{K}_2 - \cos \frac{\theta}{2} \sin \mathcal{K}_1 \right] \sigma_y,$$

and

$$U_2(\theta) = \cos \mathcal{K}_1 \cos \mathcal{K}_2 \quad (\text{B2})$$

$$-i \left[-\cos \frac{\theta}{2} \sin \mathcal{K}_1 \cos \mathcal{K}_2 + \sin \frac{\theta}{2} \sin \mathcal{K}_2 \right] \sigma_x$$

$$-i \left[-\sin \frac{\theta}{2} \sin \mathcal{K}_1 \cos \mathcal{K}_2 - \cos \frac{\theta}{2} \sin \mathcal{K}_2 \right] \sigma_y,$$

By setting $\cos[E(\theta)] = \cos \mathcal{K}_1 \cos \mathcal{K}_2$, it is straightforward to see that $E(\theta) = \arccos(\cos \mathcal{K}_1 \cos \mathcal{K}_2)$, and Eqs. (B1) and (B2) has the form of Eq. (10) in the main text, with

$$n_{1x} = \frac{+\cos \frac{\theta}{2} \cos \mathcal{K}_1 \sin \mathcal{K}_2 + \sin \frac{\theta}{2} \sin \mathcal{K}_1}{\sin E(\theta)}, \quad (\text{B3})$$

$$n_{1y} = \frac{+\sin \frac{\theta}{2} \cos \mathcal{K}_1 \sin \mathcal{K}_2 - \cos \frac{\theta}{2} \sin \mathcal{K}_1}{\sin E(\theta)}, \quad (\text{B4})$$

$$n_{2x} = \frac{-\cos \frac{\theta}{2} \sin \mathcal{K}_1 \cos \mathcal{K}_2 + \sin \frac{\theta}{2} \sin \mathcal{K}_2}{\sin E(\theta)}, \quad (\text{B5})$$

$$n_{2y} = \frac{-\sin \frac{\theta}{2} \sin \mathcal{K}_1 \cos \mathcal{K}_2 - \cos \frac{\theta}{2} \sin \mathcal{K}_2}{\sin E(\theta)}. \quad (\text{B6})$$

Appendix C: Gapless conditions

We present derivation details for the gap closing conditions. Using shorthand notations

$$\mathbf{u}_1 \equiv u_1 \sin \frac{\theta}{2}, \quad \mathbf{u}_2 \equiv u_2 \cos \frac{\theta}{2}, \quad (\text{C1})$$

$$\mathbf{v}_1 \equiv v_1 \sin \frac{\theta}{2}, \quad \mathbf{v}_2 \equiv v_2 \cos \frac{\theta}{2}, \quad (\text{C2})$$

we can express the gap closing condition as

$$\cos E = \cos(\mathbf{u}_1 + i \mathbf{v}_1) \cos(\mathbf{u}_2 + i \mathbf{v}_2) = \pm 1. \quad (\text{C3})$$

When $v_1 \neq 0$ and $v_2 = 0$, this condition is equivalent to:

$$\cos \mathbf{u}_1 \cosh \mathbf{v}_1 \cos \mathbf{u}_2 = \pm 1, \quad (\text{C4})$$

$$\sin \mathbf{u}_1 \sinh \mathbf{v}_1 \cos \mathbf{u}_2 = 0. \quad (\text{C5})$$

It is clear that to satisfy both of the equations, $\cos \mathbf{u}_2$ cannot be zero. Furthermore, if $\sinh \mathbf{v}_1 = 0$, we must have $\sin \frac{\theta}{2} = 0$, and Eq. (C5) will be satisfied only if $\cos(\mathbf{u}_2) = \pm 1$, which is a very special condition that is irrelevant to the value of v_1 . Therefore, Eq. (C5) is generally satisfied if $\sin \mathbf{u}_1 = 0$, yielding $\sin \frac{\theta}{2} = \frac{n\pi}{u_1}$ for $n\pi \leq u_1$ with $n \in \mathbb{N}$. Plugging this relation into Eq.

(C4) and regroup the relevant terms, we obtain Eq. (14) in the main text. Eq. (15) can be derived in a similar manner.

In more general situations, the gapless condition can be extracted numerically. We first separate Eq. (C3) into its real part f and imaginary part g . Expressed in terms of f and g , the Floquet spectrum is gapless when

$$\begin{aligned} \pm 1 = f &= \cos u_1 \cos u_2 \cosh v_1 \cosh v_2 \\ &- \sin u_1 \sin u_2 \sinh v_1 \sinh v_2, \end{aligned} \quad (C6)$$

and

$$\begin{aligned} 0 = g &= \cos u_1 \sin u_2 \cosh v_1 \sinh v_2 \\ &+ \sin u_1 \cos u_2 \sinh v_1 \cosh v_2. \end{aligned} \quad (C7)$$

Using f and g , we could further introduce a pair of functions (Δ_0, Δ_π) to characterize the size of spectrum gaps at quasienergy $E = 0$ and $E = \pm\pi$, respectively. Explicitly, these functions are defined as

$$\Delta_0 = \sqrt{(f-1)^2 + g^2}, \quad (C8)$$

$$\Delta_\pi = \sqrt{(f+1)^2 + g^2}. \quad (C9)$$

Therefore, the spectrum becomes gapless at the center (edge) of the quasienergy Brillouin zone if $\Delta_0 = 0$ ($\Delta_\pi = 0$).

Appendix D: Derivation of the mean chiral displacement

We provide derivation details for Eq. (17) in this appendix. In the definition of chiral displacement by Eq. (16), we can insert the identity in lattice representation to yield

$$\begin{aligned} \text{Tr} \left(\rho_0 \hat{U}_\alpha^{\dagger t} (\hat{n} \otimes \Gamma) \hat{U}_\alpha^t \right) &= \frac{1}{2} \sum_n \sum_{s,s'=a,b} \\ &\times n \langle 0 | \langle s | \hat{U}_\alpha^{\dagger t} | n \rangle \Gamma | s' \rangle \langle s' | \langle n | \hat{U}_\alpha^t | 0 \rangle | s \rangle. \end{aligned} \quad (D1)$$

Expressing \hat{U}_α and \hat{U}_α^\dagger in quasiposition (or quasimomentum for real space lattices) representation as $\hat{U}_\alpha = \sum_\theta |\theta\rangle U_\alpha(\theta) \langle \theta|$ and $\hat{U}_\alpha^\dagger = \sum_\theta |\theta\rangle \tilde{U}_\alpha^\dagger(\theta) \langle \theta|$, with $U_\alpha(\theta)$ and $\tilde{U}_\alpha^\dagger(\theta)$ being 2×2 matrices in the sublattice representation, we further obtain

$$\begin{aligned} \text{Tr} \left(\rho_0 \hat{U}_\alpha^{\dagger t} (\hat{n} \otimes \Gamma) \hat{U}_\alpha^t \right) &= \frac{1}{2} \sum_n \sum_{\theta\theta'} n \\ &\times \langle 0 | \theta \rangle \langle \theta | n \rangle \langle n | \theta' \rangle \langle \theta' | 0 \rangle \text{Tr} \left[\tilde{U}_\alpha^{\dagger t}(\theta) \Gamma U_\alpha^t(\theta') \right], \end{aligned} \quad (D2)$$

where the trace is now taken over the sublattice degrees of freedom. Using the Fourier transform relations

$$\begin{aligned} |\theta\rangle &= \frac{1}{\sqrt{N}} \sum_n e^{i\theta n} |n\rangle, \\ |n\rangle &= \frac{1}{\sqrt{N}} \sum_\theta e^{-i\theta n} |\theta\rangle, \\ \langle n | \theta \rangle &= \frac{1}{\sqrt{N}} e^{i\theta n}, \end{aligned} \quad (D3)$$

we can simplify the numerator to

$$\begin{aligned} \text{Tr} \left(\rho_0 \hat{U}_\alpha^{\dagger t} (\hat{n} \otimes \Gamma) \hat{U}_\alpha^t \right) &= \frac{1}{2} \sum_n \sum_{\theta\theta'} n \\ &\times \frac{1}{N^2} e^{in(\theta' - \theta)} \text{Tr} \left[\tilde{U}_\alpha^{\dagger t}(\theta) \Gamma U_\alpha^t(\theta') \right], \end{aligned} \quad (D4)$$

Using the relation

$$\frac{1}{N} \sum_n n e^{i(\theta' - \theta)n} = i \partial_\theta \frac{1}{N} \sum_n e^{i(\theta' - \theta)n} = i \partial_\theta \delta_{\theta\theta'}, \quad (D5)$$

we find

$$\begin{aligned} \text{Tr} \left(\rho_0 \hat{U}_\alpha^{\dagger t} (\hat{n} \otimes \Gamma) \hat{U}_\alpha^t \right) &= \frac{1}{2} \sum_{\theta\theta'} \\ &\times \frac{1}{N} i \partial_\theta \delta_{\theta\theta'} \text{Tr} \left[\tilde{U}_\alpha^{\dagger t}(\theta) \Gamma U_\alpha^t(\theta') \right], \end{aligned} \quad (D6)$$

In the continuous limit ($N \rightarrow \infty$), we have $\delta_{\theta\theta'} \rightarrow \frac{2\pi}{N} \delta(\theta - \theta')$ and $\sum_{\theta,\theta'} \rightarrow N^2 \int_{-\pi}^{\pi} \frac{d\theta}{2\pi} \int_{-\pi}^{\pi} \frac{d\theta'}{2\pi}$. Combining this into the Eq. (D6) above then leads to

$$\begin{aligned} C_\alpha(t) &= \text{Tr} \left(\rho_0 \hat{U}_\alpha^{\dagger t} (\hat{n} \otimes \Gamma) \hat{U}_\alpha^t \right) \\ &= \frac{1}{2} \int_{-\pi}^{\pi} \frac{d\theta}{2\pi} \text{Tr} \left[\tilde{U}_\alpha^{\dagger t}(\theta) \Gamma i \partial_\theta U_\alpha^t(\theta) \right]. \end{aligned} \quad (D7)$$

Inserting the normalization factor $\frac{1}{2} \text{Tr} \left[\tilde{U}_\alpha^{\dagger t}(\theta) U_\alpha^t(\theta) \right]$ at each θ (since the evolution will change the normal of the state), and taking the long time average $\lim_{t \rightarrow \infty} \frac{1}{t} \sum_{t'=1}^t$, we obtain the expression for MCD as

$$\bar{C}_\alpha = \lim_{t \rightarrow \infty} \frac{1}{t} \sum_{t'=1}^t \int_{-\pi}^{\pi} \frac{d\theta}{2\pi} \frac{\text{Tr} \left[\tilde{U}_\alpha^{\dagger t'}(\theta) \Gamma i \partial_\theta U_\alpha^{t'}(\theta) \right]}{\text{Tr} \left[\tilde{U}_\alpha^{\dagger t'}(\theta) U_\alpha^{t'}(\theta) \right]} \quad (D8)$$

For the NH-ORDKR, we have $\Gamma = \sigma_z$, $U_\alpha(\theta) = e^{-iE(\mathbf{n}_\alpha \cdot \boldsymbol{\sigma})}$ and $\tilde{U}_\alpha^\dagger(\theta) = e^{+iE^*(\mathbf{n}_\alpha \cdot \boldsymbol{\sigma})}$. Plugging these into

Eq. (D8), the numerator and denominator become

$$\text{Tr} \left[\tilde{U}_\alpha^{\dagger t'}(\theta) U_\alpha^{t'}(\theta) \right] = 2 \left[|\cos(Et')|^2 + |\sin(Et')|^2 \right] \quad (\text{D9})$$

$$\text{Tr} \left[\tilde{U}_\alpha^{\dagger t'}(\theta) \Gamma i \partial_\theta U_\alpha^{t'}(\theta) \right] = 2 |\sin(Et')|^2 (\mathbf{n}_\alpha \times \partial_\theta \mathbf{n}_\alpha)_z \quad (\text{D10})$$

Combining these into Eq. (D8), we finally obtain Eq. (17) in the main text.

-
- [1] P. Leboeuf, J. Kurchan, M. Feingold, and D. P. Arovas, Phys. Rev. Lett. **65**, 3076 (1990).
- [2] G. Casati, B.V. Chirikov, F.M. Izrailev and J. Ford, in *Stochastic Behaviour in classical and Quantum Hamiltonian Systems*, Vol. **93** of Lecture Notes in Physics, edited by G. Casati and J. Ford (Springer, New York, 1979).
- [3] G. Casati and B. V. Chirikov, *Quantum Chaos: Between Order and Disorder* (Cambridge University Press, New York, 1995).
- [4] H. Ammann, R. Gray, I. Shvarchuck, and N. Christensen, Phys. Rev. Lett. **80**, 4111 (1998); B. G. Klappauf, W. H. Oskay, D. A. Steck, and M. G. Raizen, Phys. Rev. Lett. **81**, 1203 (1998).
- [5] J. Chabé, G. Lemarié, B. Grémaud, D. Delande, P. Szriftgiser, and J. C. Garreau, Phys. Rev. Lett. **101**, 255702 (2008).
- [6] D. H. White, S. K. Ruddell, and M. D. Hoogerland, Phys. Rev. A **88**, 063603 (2013).
- [7] F. M. Izrailev, Phys. Rep. **196**, 299 (1990); M. G. Raizen, Advances In Atomic, Molecular, and Optical Physics **41**, 43 (1999); I. Dana, Can. J. Chem. **92**, 77 (2014); M. Sadgrovea and S. Wimberger, Advances in Atomic, Molecular, and Optical Physics **60**, 315 (2011).
- [8] J. Wang and J. B. Gong, Phys. Rev. A **77**, 031405 (2008); J. Wang, A. S. Mouritzen, and J. Gong, J. Mod. Optics **56**, 722 (2009).
- [9] D. R. Hofstadter, Phys. Rev. B **14**, 2239 (1976).
- [10] D.Y.H. Ho and J. Gong, Phys. Rev. Lett. **109**, 010601 (2012); D.Y.H. Ho and J. Gong, Phys. Rev. B **90**, 195419 (2014).
- [11] I. Dana, Phys. Lett. A **197**, 413 (1995).
- [12] H. Wang, D. Y. H. Ho, W. Lawton, J. Wang, and J. Gong, Phys. Rev. E **88**, 052920 (2013).
- [13] J. P. Dahlhaus, J. M. Edge, J. Tworzydło, and C. W. J. Beenakker, Phys. Rev. B **84**, 115133 (2011).
- [14] Y. Chen and C. Tian, Phys. Rev. Lett. **113**, 216802 (2014); C. Tian, Y. Chen, and J. Wang, Phys. Rev. B **93**, 075403 (2016).
- [15] L. Zhou and J. Gong, Phys. Rev. A **97**, 063603 (2018).
- [16] T. Oka and H. Aoki, Phys. Rev. B **79**, 081406 (2009).
- [17] N. H. Lindner, G. Refael, and V. Galitski, Nat. Phys. **7**, 490 (2011).
- [18] T. Kitagawa, T. Oka, A. Brataas, L. Fu, and E. Demler, Phys. Rev. B **84**, 235108 (2011).
- [19] Q.-J. Tong, J.-H. An, J. Gong, H.-G. Luo, and C. H. Oh, Phys. Rev. B **87**, 201109 (2013).
- [20] L. Zhou, H. Wang, D. Y. H. Ho, and J. Gong, Eur. Phys. J. B **87**, 204 (2014).
- [21] T.-S. Xiong, J. Gong, and J.-H. An, Phys. Rev. B **93**, 184306 (2016).
- [22] Á. Gómez-León and G. Platero, Phys. Rev. Lett. **110**, 200403 (2013).
- [23] J. Cayssol, B. Dóra, F. Simon, and R. Moessner, Phys. Status Solidi Rapid Res. Lett. **7**, 101 (2013).
- [24] M. Thakurathi, A. A. Patel, D. Sen and A. Dutta, Phys. Rev. B **88**, 155133 (2013).
- [25] A. G. Grushin, Á. Gómez-León, and T. Neupert, Phys. Rev. Lett. **112**, 156801 (2014).
- [26] R. Wang, B. Wang, R. Shen, L. Sheng, and D. Y. Xing, Europhys. Lett. **105**, 17004 (2014).
- [27] P. Titum, N. H. Lindner, M. C. Rechtsman, and G. Refael, Phys. Rev. Lett. **114**, 056801 (2015).
- [28] J. Klinovaja, P. Stano, and D. Loss, Phys. Rev. Lett. **116**, 176401 (2016); M. Thakurathi, D. Loss, and J. Klinovaja, Phys. Rev. B **95**, 155407 (2017).
- [29] T. Kitagawa, E. Berg, M. Rudner, and E. Demler, Phys. Rev. B **82**, 235114 (2010).
- [30] L. Jiang, T. Kitagawa, J. Alicea, A. R. Akhmerov, D. Pekker, G. Refael, J. I. Cirac, E. Demler, M. D. Lukin, and P. Zoller, Phys. Rev. Lett. **106**, 220402 (2011).
- [31] A. Kundu and B. Seradjeh, Phys. Rev. Lett. **111**, 136402 (2013).
- [32] R. W. Bomantara, G. N. Raghava, L. Zhou, and J. Gong, Phys. Rev. E **93**, 022209 (2016); R. W. Bomantara and J. Gong, Phys. Rev. B **94**, 235447 (2016).
- [33] M. Lababidi, I. I. Satija, and E. Zhao, Phys. Rev. Lett. **112**, 026805 (2014); Z. Zhou, I. I. Satija, and E. Zhao, Phys. Rev. B **90**, 205108 (2014).
- [34] M. D. Reichl and E. J. Mueller, Phys. Rev. A **89**, 063628 (2014).
- [35] Á. Gómez-León, P. Delplace, and G. Platero, Phys. Rev. B **89**, 205408 (2014).
- [36] M. S. Rudner, N. H. Lindner, E. Berg, and M. Levin, Phys. Rev. X **3**, 031005 (2013); P. Titum, E. Berg, M. S. Rudner, G. Refael, and N. H. Lindner, Phys. Rev. X **6**, 021013 (2016).
- [37] I. C. Fulga and M. Maksymenko, Phys. Rev. B **93**, 075405 (2016).
- [38] L. Zhou, C. Chen, and J. Gong, Phys. Rev. B **94**, 075443 (2016).
- [39] J. K. Asbóth, Phys. Rev. B **86**, 195414 (2012); J. K. Asbóth, and H. Obuse, Phys. Rev. B **88**, 121406 (2013).
- [40] M. Rodríguez-Vega and B. Seradjeh, Phys. Rev. Lett. **121**, 036402 (2018).
- [41] H. H. Yap, L. Zhou, J. Wang, and J. Gong, Phys. Rev.

- B **96**, 165443 (2017).
- [42] H. H. Yap, L. Zhou, C. H. Lee, J. Gong, Phys. Rev. B **97**, 165142 (2018).
- [43] L. Zhou and J. Gong, Phys. Rev. B **97**, 245430 (2018).
- [44] L. Li, C. H. Lee, and J. Gong, Phys. Rev. Lett. **121**, 036401 (2018).
- [45] T. Oka, and S. Kitamura, Annu. Rev. Condens. Matter Phys. **10**, 387 (2019).
- [46] A. Eckardt, Rev. Mod. Phys. **89**, 011004 (2017).
- [47] R.W. Bomantara and J. Gong, Phys. Rev. Lett. **120**, 230405 (2018). R.W. Bomantara and J. Gong, Phys. Rev. B **98**, 165421 (2018).
- [48] F. Nathan and M. S. Rudner, New J. Phys. **17**, 125014 (2015).
- [49] R. Roy and F. Harper, Phys. Rev. B **94**, 125105 (2016); R. Roy and F. Harper, Phys. Rev. B **96**, 155118 (2017).
- [50] S. Yao, Z. Yan, and Z. Wang, Phys. Rev. B **96**, 195303 (2017).
- [51] G. Jotzu, M. Messer, R. Desbuquois, M. Lebrat, T. Uehlinger, D. Greif, and T. Esslinger, Nature **515**, 237 (2014); M. Aidelsburger, M. Lohse, C. Schweizer, M. Atala, J. T. Barreiro, S. Nascimbène, N. R. Cooper, I. Bloch and N. Goldman, Nat. Phys. **11**, 162 (2015).
- [52] N. Fläschner, B. S. Rem, M. Tarnowski, Vogel, D.-S. Lühmann, K. Sengstock, and C. Weitenberg, Science **352**, 1091 (2016).
- [53] T. Kitagawa, M. A. Broome, A. Fedrizzi, M. S. Rudner, E. Berg, I. Kassal, A. Aspuru-Guzik, E. Demler and A. G. White, Nat. Commun. **3**, 882 (2012).
- [54] M. C. Rechtsman, J. M. Zeuner, Y. Plotnik, Y. Lumer, D. Podolsky, F. Dreisow, S. Nolte, M. Segev, and A. Szameit, Nature **496**, 196 (2013); W. Hu, J. C. Pillay, K. Wu, M. Pasek, P. P. Shum, and Y. D. Chong, Phys. Rev. X **5**, 011012 (2015).
- [55] L. J. Maczewsky, J. M. Zeuner, S. Nolte, and A. Szameit, Nat. Commun. **8**, 13756 (2017); S. Mukherjee, A. Spracklen, M. Valiente, E. Andersson, P. Ohberg, N. Goldman, and R. R. Thomson, Nat. Commun. **8**, 13918 (2017).
- [56] M. Xiao, G. Ma, Z. Yang, P. Sheng, Z. Q. Zhang, and C. T. Chan, Nat. Phys. **11**, 240 (2015); R. Süssstrunk and S. D. Huber, Science **349**, 47 (2015); R. Fleury, A. B. Khanikaev and A. Alù, Nat. Commun. **7**, 11744 (2016); R. Süssstrunk, P. Zimmermann, and S. D. Huber, New J. Phys. **19**, 015013 (2017).
- [57] Y. Peng, C. Qin, D. Zhao, Y. Shen, X. Xu, M. Bao, H. Jia, and X. Zhu, Nat. Commun. **7**, 13368 (2016).
- [58] V. M. M. Alvarez, J. E. B. Vargas, M. Berdakin, and L. E. F. Foa Torres, Eur. Phys. J. Special Topics **227**, 1295 (2018).
- [59] A. Ghatak, and T. Das, J. Phys.: Condens. Matter **31**, 263001 (2019); A. Ghatak, and T. Das, arXiv:1907.07333 (2019).
- [60] C. Yuce, The European Physical Journal D **69**, 184 (2015); Z. Turker, S. Tombuloglu, and C. Yuce, Phys. Lett. A **382**, 2013 (2018).
- [61] D. Kim, M. Ken, N. Kawakami, H. Obuse, arXiv:1609.09650 (2016).
- [62] J. Gong and Q. Wang, Phys. Rev. A **91**, 042135 (2015).
- [63] X. Lü, H. Jing, J. Ma, and Y. Wu, Phys. Rev. Lett. **114**, 253601 (2015).
- [64] Q. Bin, X. Lü, T. Yin, Y. Li, and Y. Wu, Phys. Rev. A **99**, 033809 (2019).
- [65] M. S. Rudner and L. S. Levitov, Phys. Rev. Lett. **102**, 65703 (2009).
- [66] J. M. Zeuner, M. C. Rechtsman, Y. Plotnik, Y. Lumer, S. Nolte, M. S. Rudner, M. Segev, and A. Szameit, Phys. Rev. Lett. **115**, 40402 (2015).
- [67] K. Mochizuki, D. Kim, and H. Obuse, Phys. Rev. A **93**, 062116 (2016).
- [68] Y. Huang, Z. Yin, and W. L. Yang, Phys. Rev. A **94**, 022302 (2016).
- [69] T. Rakovszky, J. K. Asbóth, and A. Alberti, Phys. Rev. B **95**, 201407 (2017).
- [70] L. Xiao, X. Zhan, Z. H. Bian, K. K. Wang, X. Zhang, X. P. Wang, J. Li, K. Mochizuki, D. Kim, N. Kawakami, W. Yi, H. Obuse, B. C. Sanders, and P. Xue, Nat. Phys. **13**, 1117 (2017); L. Xiao, X. Qiu, K. Wang, Z. Bian, X. Zhan, H. Obuse, B. C. Sanders, W. Yi, and P. Xue, Phys. Rev. A **98**, 063847 (2018).
- [71] T. Chen, B. Wang, and X. Zhang, Phys. Rev. A **97**, 052117 (2018).
- [72] A. K. Harter, A. Saxena, and Y. N. Joglekar, Sci. Rep. **8**, 12065 (2018).
- [73] K. Wang, X. Qiu, L. Xiao, X. Zhan, Z. Bian, W. Yi, and P. Xue, Phys. Rev. Lett. **122**, 020501 (2019).
- [74] L. Zhou, and J. Gong, Phys. Rev. B **98**, 205417 (2018).
- [75] S. Longhi, Phys. Rev. A **95**, 012125 (2017).
- [76] C. T. West, T. Kottos, and T. Prosen, Phys. Rev. Lett. **104**, 054102 (2010).
- [77] W. Zhao, J. Wang, X. Wang, and P. Tong, Phys. Rev. E **99**, 042201 (2019).
- [78] P. H. Jones, M. M. Stocklin, G. Hur, and T. S. Monteiro, Phys. Rev. Lett. **93**, 223002 (2004).
- [79] G. Hur, C. E. Creffield, P. H. Jones, and T. S. Monteiro, Phys. Rev. A **72**, 013403 (2005); C. E. Creffield, S. Fishman, and T. S. Monteiro, Phys. Rev. E **73**, 066202 (2006); M. M. A. Stocklin and T. S. Monteiro, Phys. Rev. E **74**, 026210 (2006); C. E. Creffield, G. Hur, and T. S. Monteiro, Phys. Rev. Lett. **96**, 024103 (2006); J. Reslen, C. E. Creffield, and T. S. Monteiro, Phys. Rev. A **77**, 043621 (2008).
- [80] G. G. Carlo, G. Benenti, G. Casati, S. Wimberger, O. Morsch, R. Mannella, and E. Arimondo, Phys. Rev. A **74**, 033617 (2006).
- [81] C. Ryu, M. F. Andersen, A. Vaziri, M. B. d'Arcy, J. M. Grossman, K. Helmerson, and W. D. Phillips, Phys. Rev. Lett. **96**, 160403 (2006); I. Talukdar, R. Shrestha, and G. S. Summy, Phys. Rev. Lett. **105**, 054103 (2010).
- [82] I. Dana, V. Ramareddy, I. Talukdar, and G. S. Summy, Phys. Rev. Lett. **100**, 024103 (2008); M. Sadgrove, M. Horikoshi, T. Sekimura, and K. Nakagawa, Phys. Rev. Lett. **99**, 043002 (2007).
- [83] F. L. Moore, J. C. Robinson, C. F. Bharucha, B. Sundaram, and M. G. Raizen, Phys. Rev. Lett. **75**, 4598 (1995); J. F. Kanem, S. Maneshi, M. Partlow, M. Spanner, and A. M. Steinberg, Phys. Rev. Lett. **98**, 083004 (2007); A. Ullah and M. D. Hoogerland, Phys. Rev. E **83**, 046218 (2011).
- [84] Y. Xu, S. Wang, and L.-M. Duan, Phys. Rev. Lett. **118**, 045701 (2017).
- [85] S. Longhi, Phys. Rev. A **81**, 022102 (2010).
- [86] In calculations, we take absolute values on the right-hand side of Eq. (13) to compute (ν_0, ν_π) . In topological sense, $\nu_0 = \pm 1$ do not distinguish two different topological phases. The sign of a winding number could depend on the choice of conventions.
- [87] F. Cardano, A. D'Errico, A. Dauphin, M. Maffei, B. Pic-

- cirillo, C. de Lisio, G. D. Filippis, V. Cataudella, E. Santamato, L. Marrucci, M. Lewenstein and P. Massignan, Nat. Commun. **8**, 15516 (2017); M. Maffei, A. Dauphin, F. Cardano, M. Lewenstein and P. Massignan, New J. Phys. **20**, 013023 (2018).
- [88] E. J. Meier, F. A. An, A. Dauphin, M. Maffei, P. Massignan, T. L. Hughes, and B. Gadway, Science **362**, 929 (2018).
- [89] R.W. Bomantara, L.Zhou, J. Pan, and J. Gong, Phys. Rev. B **99**, 045441 (2019).
- [90] F. K. Kunst, E. Edvardsson, J. C. Budich, and E. J. Bergholtz, Phys. Rev. Lett. **121**, 026808 (2018).
- [91] D. S. Borgnia, A. J. Kruchkov, and R. Slager, arXiv:1902.07217 (2019).
- [92] T.E. Lee, Phys. Rev. Lett. **116**, 133903 (2016).
- [93] D. J. Luitz and F. Piazza, Phys. Rev. Research **1**, 033051 (2019).
- [94] S. Yao and Z. Wang, Phys. Rev. Lett. **121**, 086803 (2018).
- [95] L. Xiao, T. Deng, K. Wang, G. Zhu, Z. Wang, W. Yi, and P. Xue, arXiv:1907.12566 (2019).
- [96] X. Zhang and J. Gong, arXiv:1909.10234 (2019).
- [97] H. Zhou, and J. Y. Lee, Phys. Rev. B **99**, 235112 (2019).
- [98] K. Kawabata, K. Shiozaki, M. Ueda, and M. Sato, arXiv:1812.09133 (2018).
- [99] L. Zhou, arXiv:1909.10797 (2019).
- [100] S. Tan, R. W. Bomantara, and J. Gong, arXiv:1909.03646 (2019).